Check for updates

Synthesis of a hydrophobic associating polymer and its application in plugging spacer fluid

Zhaofeng Xue,[ab] Miaomiao Hu,*[ab] Xia Miao,[c] Long Zang[ab] and Jintang Guo [ID] *[ab]

The high temperature of formation and multiple stages of leakage zone seriously affect the efficiency and safety of drilling and cementing operations. To improve leakage plugging quality before the cementing process, the hydrophobic associating polymer PHAAO was synthesized from acrylamide (AM), 2-acrylamide-2-methyl propane sulfonic acid (AMPS), and the long side-chain hydrophobic monomer octadecyl dimethyl allyl ammonium chloride (ODAAC) in this study. The structure and molecular weight of the polymer were characterized, and it was proved that the polymer has strong association properties and excellent heat resistance. Utilizing the bridge plugging principle, the polymer PHAAO was used with 36-mesh walnut shells and lignin fiber to form a compound plugging agent. This agent was added to spacer fluid to become a plugging spacer. API water loss tests and loading capacity tests under high temperatures show that the filter cake formed by the spacer fluid is dense. The sealing pressure of the spacer fluid on a 1 mm crack can reach 6.5 MPa at 160 °C, and it has good compatibility with cement slurry. A scanning electron microscopy (SEM) test was conducted to explore the membrane formation mechanism of the polymer. An ultra-low permeability membrane is formed on the surface of the filter cake from the spacer fluid due to the hydrophobic association and hydrogen bonding between the polymer and lignin fiber, thereby greatly reducing the loss of spacer fluid.

1 Introduction

At present, there are multiple stages of leakage zones in oilfield formations, such as Permian, Silurian, and Ordovician formations, which have varying degrees of leakage during cementing. And the complex fracture distribution seriously affects the cementing quality. Meanwhile, the deep burial and high temperature (>150 °C) of the formation put forward higher requirements for the temperature resistance of cementing and leakage plugging materials. Drilling fluid plugging is more commonly used in the process of plugging, but its plugging effect is likely to fail during casing running.[1–4] Spacer fluid is a type of working fluid that is injected into the well from the casing between drilling and cement slurry being injected. The spacer fluid prevents cement contamination by flushing and displacing the drilling fluid. It can also remove mud cakes from the wellbore and strengthen the cement sheath of the formation. Therefore, plugging spacer fluid can work for a longer time and improve the success rate of plugging.

However, the research on plugging spacer fluid is far from satisfying the application requirements. For the consideration of reducing cost and environmental protection, fiber plugging

spacer fluid is advantageous. However, the requiring amount of fiber used in plugging is too much to contain excellent fluidity.

The plugging agents at the nano level achieve a good plugging effect.[5–7] Hydrophobic associating polymers is a noteworthy nanoscale plugging material, which consists of both hydrophilic segments and hydrophobic segments. In an aqueous environment, its hydrophobic groups get close and associate with each other, so that they form an association network. Due to this feature, it has been used in the ultra-low permeability drilling fluid to stable the well walls and reduce the permeability of the formation.[8–11] The mechanism can be summarized as the hydrophobic associating polymers associates on the surface of the formation and form micelles to seal the cracks. The bridge plugging agent is a kind of plugging technology often applied. Bridging particles can fill in the cracks of the pore throat to decrease the size of cracks. They are able to fill cracks by the particle size grading, but it is difficult for them to realize ultra-low permeability.

To improve plugging quality, both bearing capacity and reducing fluid loss need to be taken into consideration. Combining hydrophobic associating polymer with the bridge plugging material is a promising method to achieve high-pressure resistance, high-temperature resistance, plug large cracks, and ultra-low permeability at the same time.

Herein, the high-temperature resistant monomer and the large hydrophobic monomer with 18 carbon atoms in the side chain were selected, and the polymer with good temperature

[a]School of Chemical Engineering and Technology, Tianjin University, Tianjin 300350, China. E-mail: mmhu1990@tju.edu.cn; jtguo@tju.edu.cn

[b]Institute of Shaoxing, Tianjin University, Zhejiang, 312300, China

[c]Sinopec Research Institute of Petroleum Engineering, Beijing 102206, China

resistance and strong hydrophobic association was synthesized by AM, AMPS and ODAAC using simple aqueous micelle free radical polymerization. The structure and properties of the polymer were characterized. It was combined with lignin fiber which is of good toughness, dispersibility and high strength as well as with 36 mesh walnut shells which are of high compressive strength and chemical inertia. The comprehensive performance of the isolation fluid with the plugging agent was verified by a series of experiments. The surface morphology of the filter cake was observed by scanning electron microscope, and the mechanism of ultra-low permeability was revealed.

2 Experimental section

2.1 Materials

Acrylamide (AM), 2-Acrylamido-2-Methyl-Propane sulfonic Acid (AMPS), ammonium persulfate (APS) and deuterium aqueous solvent (D_2O) were purchased from Aladdin Industrial Cooperation, octadecyl dimethyl allyl ammonium chloride (ODAAC) was purchased from Jiangsu Feymer Technology Co. Ltd. Potassium bromide used of the Scanned by Fourier transform infrared spectroscopy is spectrography (purity $\geq$ 99.9%) and it was purchased from Tianjin Kemiou Chemical Reagent Co., LTD. OP-10 (surfactant) was purchased from Shandong Polymer Co., Ltd. Jiahua G grade oil well cement (high sulfate-resistant type) was purchased from Sichuan Leshan Jiahua Cement Factory. Lignin fiber was purchased from Changzhou Zhuwei Building Materials Co., LTD. The walnut shell was purchased from Gongyi Hengfeng Environmental Protection Technology Co., LTD. Barite comes from Chengdu Omec Petroleum Technology Co., LTD. Retarder, water loss reducer and suspension stabilizer were purchased from Weihui Chemical Co., LTD.

2.2 Preparation of hydrophobic associating polymer

The polymerization method is the micelle free-radical aqueous solution polymerization. AMPS was dissolved in water, and sodium hydroxide was added with a pH meter stirring to adjust the pH value in the range of 5–6. AM was dissolved in water, and ODAAC was dissolved in a certain concentration aqueous solution of the emulsifier OP-10. The above three aqueous solutions were mixed and stirred evenly. The mixed solution was poured into a three-mouth flask and the initiator, ammonium persulfate (APS), was added to the three-mouth flask when the temperature of the water bath was 70 °C. The reaction continued for 4 h under the condition of mechanical agitation. The viscous transparent polymer PHAAO solution was obtained ultimately.

2.3 Structural characterization of polymers

2.3.1 Molecular structure characterization. PHAAO polymer was purified by dialysis membrane with molecular retention of 3500 Da. Then the PHAAO sample was stirred in deionized water for 72 h and the solid polymer was obtained after being refrigerated for 10 h and vacuumize for 72 h at −40 °C which vacuum degree is 15 Pa. The molecular structure of PHAAO was scanned by Fourier transform infrared

spectroscopy (FTIR)(Bio-RAD FTS 3000, Bruker Daltonic Inc, USA). Then, the polymer PHAAO was dissolved in deuterium oxide (D_2O) and characterized by hydrogen nuclear magnetic resonance (^{1}H NMR spectrometer) (AVANCE III 400, Bruker, Switzerland). Multi-detection gel chromatography (TDA305, Malvern Instruments Co. Ltd, Britain) with 2414RI Detector and Waters e2695 separations module was used to measure the molecular weight of the polymer. The mobile phase was sodium nitrate solution (0.1 mol L^{-1}, 0.5 mL min^{-1}). The column size was 300×8.0 mm and its temperature was 35 °C. The standard sample was polyethylene glycol. To calculate the M_w of the polymer, the retention time of the polymer sample was pinpointed, and the corresponding molecular weight could be found on the gel permeation chromatography curve of the standard sample.

2.3.2 Characterization of hydrophobic association structure. The hydrophobic micro-regions of PHAAO were determined by fluorescence probe and ultraviolet spectrophotometer.[12,13] The purified solid polymer was dissolved in quantitative deionized water and polymer solutions with different concentrations were obtained. The quantitative pyrene probe was added to the polymer solutions. A fluorescence spectrophotometer (F-2500, Hitachi, Japan) was used to analyze the fluorescence spectrum of the samples. Ultraviolet absorption intensity was measured by ultraviolet spectrophotometer (UV-1800, Shimadzu, Japan).

2.3.3 Critical association concentration test. The critical association concentration of the polymer was measured using a viscosimeter (DV-II, Brookfield, USA) with a No. 0 rotor. The method to calculate the M_{wt} of the polymer is as followed:

$$wt\% = \frac{m(polymer)}{m(solution)} \times 100\%$$

2.4 Dynamic light scattering analysis

The purified polymer powder with different amounts was dissolved in water and ultrasonic was performed for 30 min. After standing for 24 h, the particle size was scanned by a Malvern laser granulometry (Nano ZS, Malvern Instruments Co. Ltd, Britain).

2.5 Thermogravimetric testing of polymers

The high-temperature resistance of the purified polymer powder was tested. Dynamic thermogravimetric analysis (DTG) and thermogravimetric analysis (TGA) of samples were measured using the thermal analyzer (TGA-50 209 F3 Tarsus, Shimadzu, Japan) in the N_2 atmosphere. The heating rate is 10 °C min^{-1} and the temperature range is 30–1000 °C.

2.6 Plugging performance test

2.6.1 Ultra-low permeability test. A medium pressure water loss tester was used for the API water loss test. Take out the filter paper and filter cake after the test, and put them into the oven at 60 °C for 24 hours to dry them completely. Inject clean water into the meter, put the dried filter cake with filter paper into it. Exert pressure and time again, measure the amount of water

flowing throughout the filter cake within 30 minutes, and test the permeability of the filter cake.

2.6.2 Loading capacity test under high temperature. Use a plugging material tester to test the loading capacity of the spacer fluid at ambient temperature and high temperature, respectively. Before the high-temperature test, the roller heating furnace was used to cure the spacer fluid at 160 °C for 3 h. The width of the seam plate tested is 1 mm, and the maximum pressure of the test is 7 MPa.

2.7 Compatibility of spacer fluid and cement slurry

2.7.1 Rheological compatibility test. Rheological compatibility was tested with a twelve-speed rotational viscometer (HTD-12DST, Qingdao Tongchun Petroleum Instrument Co. Ltd, China). The rheological properties of the mixed slurry with different volume ratios of spacer fluid and cement were tested at room temperature and 93 °C respectively. The fluidity index and consistency coefficient were compared with pure cement slurry.

2.7.2 Thickening compatibility test. Dual-cylinder high temperature and high-pressure thickener (Tg-8040DA, Shenyang Taige Petroleum Instrument Manufacturing Co. Ltd, China) was used to carry out the thickening experiment. The thickening experiment was carried out at 93 °C and 30 MPa. Cement slurry and spacer fluid with different volume proportions were evenly mixed into the slurry cup of the thickener for the thickening experiment. Finally, the thickening time was compared with that of cement slurry.

2.8 Study on the mechanism of the membrane formed by polymers

The filter cake obtained from the medium pressure water loss test was dried in an oven at 60 °C for 24 h. The completely dried filter cake was taken into small pieces and glued to the conductive adhesive, sprayed with platinum powder and observed by field emission scanning electron microscopy (S-4800, Hitachi, Japan). The magnification time is 20k and the acceleration voltage is 3 kV.

3 Results and discussions

3.1 Characterization of polymers

3.1.1 Molecular structure characterization. Fig. 1 shows the Fourier transform infrared (FTIR) spectrum of polymer molecules. 3440 cm^{-1} and 1218 cm^{-1} are the stretching vibration absorption peaks of –NH and –CN in AMPS.[14] 1043 cm^{-1} and 628 cm^{-1} are ascribed to the asymmetric stretching vibration of –SO$_3$ and S–C in AMPS, respectively. 1658 cm^{-1} belongs to the stretching vibration absorption peak of the carbonyl group in AM. 2927 cm^{-1} is the asymmetric stretching vibration absorption peak of –CH$_2$ on the main chain of ODAAC, and 767 cm^{-1} is the stretching vibration absorption peak of the –CH$_2$ group on the long side chain of ODAAC. The characteristic absorption peak of C=C did not appear in the range of 1620–1640 cm^{-1}. The spectrum indicates that each monomer material was involved in the polymerization.
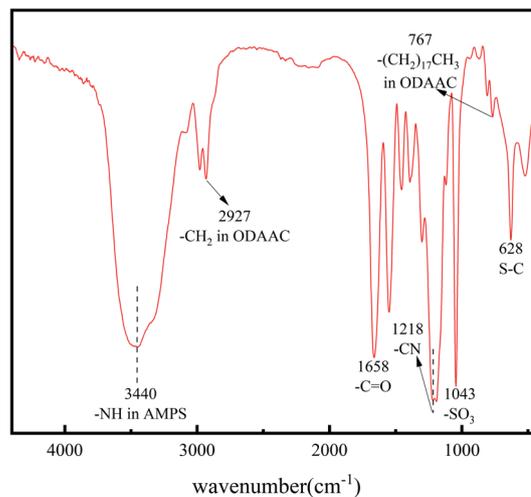

Fig. 1 FTIR spectrum of copolymer PHAAO.

To further explain the chemical structure of the polymer, the sample was analyzed by ^{1}H NMR. Fig. 2 shows the hydrogen NMR spectrum. The strong absorption peak at 4.8 ppm is the absorption peak of the D atom in D$_2$O. The peak at 3.59 ppm is the hydrogen absorption peak of methylene linked to –SO$_3$ in AMPS. The peak at 3.30 ppm belongs to the hydrogen absorption peak of the methyl group connected with N$^+$ on ODAAC. The peak at 1.27 ppm is ascribed to the hydrogen absorption peak of methylene on the long side chain of ODAAC, while the peak at 2.07 ppm and the strong peak at 1.53 ppm are the hydrogen absorption peaks of methylene and methylene on the main chain of the polymerization, respectively. The other peak at 7.5 ppm is the hydrogen absorption peak of the amide group on acrylamide. The successful synthesis of the target substance was verified by FTIR spectrum and ^{1}H NMR spectrum. Chart 1 is the molecular structure of the polymer.

Gel permeation chromatography was used to test the molecular weight of the polymer. The average molecular weight of the polymer is 54 870. The two small peaks in Fig. 3 belong to the solvent and micro-molecule in it. The molecular weight distribution PDI is 10 which is wide molecular weight distribution. It can be seen that the molecular adaptability is strong with many molecules of different sizes. The polymers can be filled into pores of different sizes.
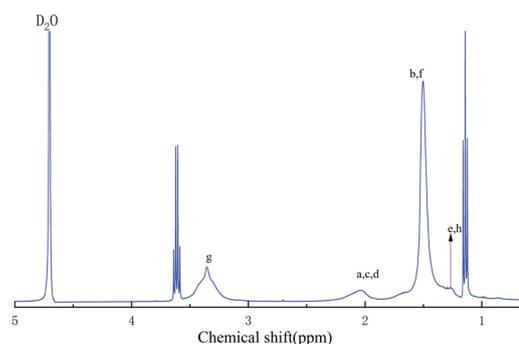

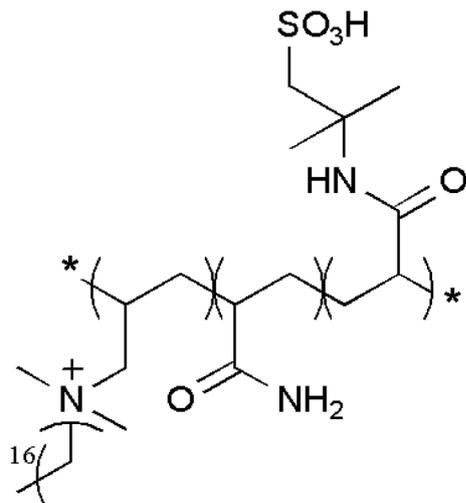Fig. 2 ^{1}H-NMR spectrum of copolymer PHAAO.

Chart 1 Molecular structure of PHAAO.

Fig. 4 Fluorescence emission spectrum of different concentration of PHAAO solution.

Fig. 5 I_3/I_1 change with PHAAO concentration.

3.1.2 Characterization of hydrophobic association structure. To fully characterize the hydrophobic association structure, the fluorescence probe method and ultraviolet spectrophotometer were used to investigate it.

There are five peaks in the emission spectrum of pyrene, as shown in Fig. 4. The change in the peak-strength ratio of I_3 and I_1 can reflect the change in the number of hydrophobic micro-regions in the system (Fig. 5). The larger I_3/I_1 is, the more non-polar regions there are in the system.[15,16] In the vicinity of the critical association concentration, the slope of this ratio will mutate.[17–20] To further confirm the hydrophobic association structure of the polymer, an ultraviolet spectrophotometer was used. The ultraviolet absorption spectrum of polymers with different concentrations are shown in Fig. 6. According to literature reports, the longest ultraviolet absorption wavelength of pyrene is 272 nm.[21–23] When the environmental polarity is weaker, the number of hydrophobic micro-regions and the ultraviolet absorption peak redshift of pyrene increases.
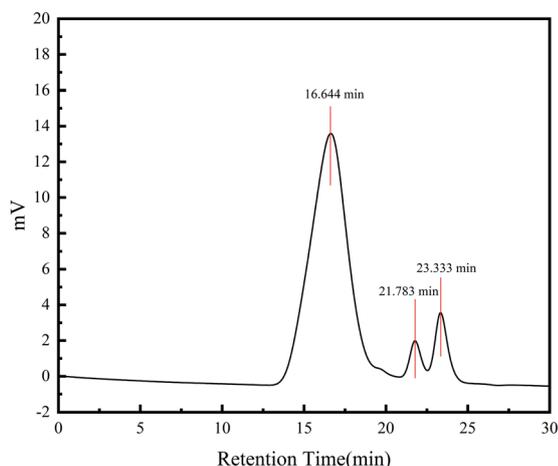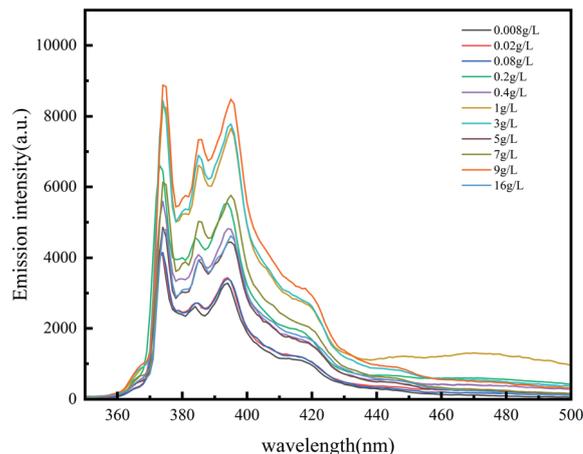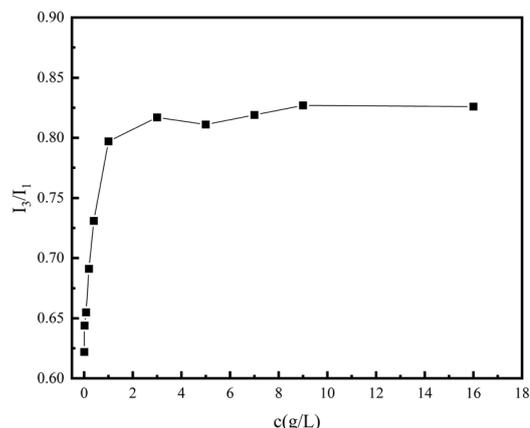
As shown in Fig. 5 and 7, when the polymer concentration is very low, the value of I_3/I_1 and the absorption wavelength shift at 272 nm are small and change rapidly with the concentration

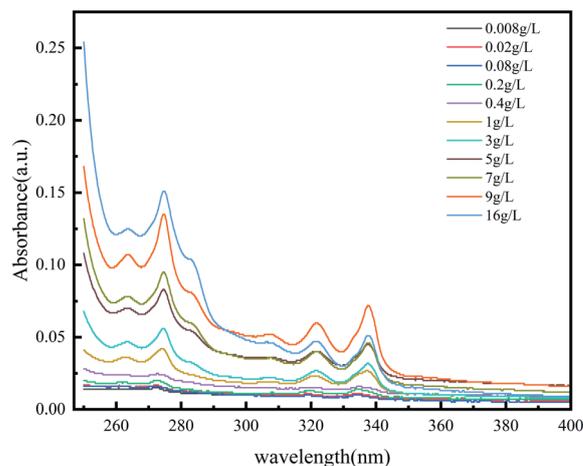**Fig. 3** Gel chromatography curve of polymer PHAAO.

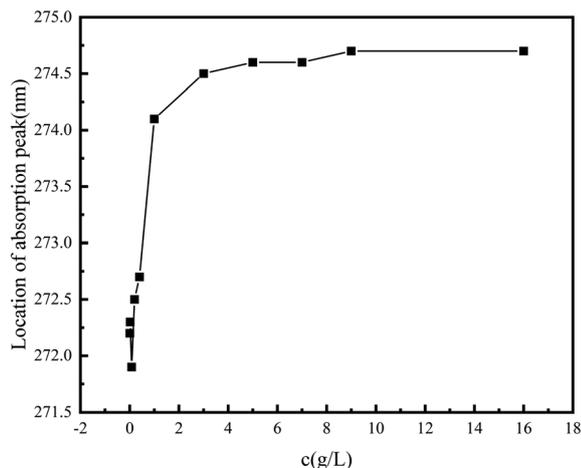**Fig. 6** Ultraviolet absorption spectrum of different PHAAO concentration.

Fig. 7 Ultraviolet absorption spectrum of different PHAAO concentration.

changing. When the concentration reaches about 0.2%, the ratio changes slowly until the ratio tends to be constant at 1%. The two turning points in the two figures correspond to the two critical association concentrations of polymers, and the change curves indicate the changes in the number of hydrophobic micro-regions. According to these two characterization results, it can be speculated that the critical association concentration of the polymer is around 1 wt%.

3.1.3 Critical association concentration test. Determining the critical association concentration of the polymer can guide the polymer addition in the spacer fluid. As can be seen from Fig. 8, when the polymer concentration is less than 1 wt%, the viscosity increases slowly with the concentration, while when the concentration is greater than 1 wt%, the viscosity changes at a sudden change rate. This is precisely because the concentration reaches the critical association concentration of the polymer. At this time, the polymer forms a large number of association structural networks in the aqueous solution, which causes the resistance of the polymer molecular chain network to
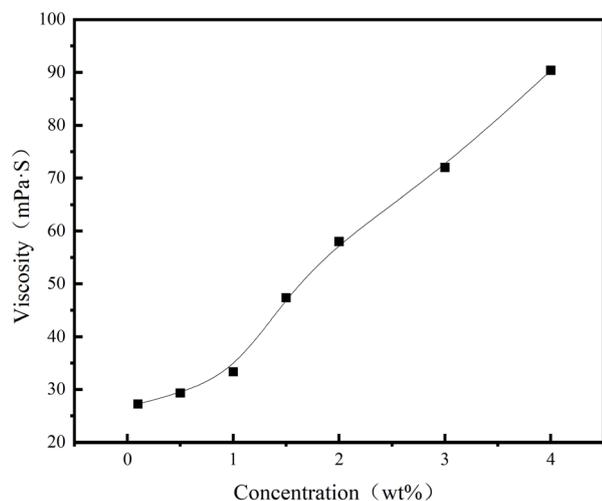
the rotating rotor in the solution and the viscosity rises rapidly.[24] Combining with the results from the fluorescence emission spectrum and UV absorption spectrum, the critical association concentration of the polymer was 1 wt%, which was inferred from the results of Section 3.1.2.

3.2 Dynamic light scattering analysis

Fig. 9 shows the dynamic light scattering diagram of the polymer aqueous solutions with a solution concentration of 0.1 wt%, 0.5 wt% and 1 wt%, respectively. The results show that with the increase of solution concentration, the scattering light intensity increases significantly when the molecular particle size is greater than 400 nm. When the critical association concentration is reached, the molecular particle size is greater than 458 nm. The particle size distribution shifted to higher molecular weight with the increase in solution concentration. Although the particle size of up to 2305 nm of molecular scattering light grabs smaller, but also exists in the solution when the concentration is only 0.1 wt%. Hydrophobic association interaction realizes the molecular aggregation obviously with the increase of solution concentration. Even if the solution concentration is lower than the critical association concentration, it also appears to have a certain association network structure. This shows that polymer molecules have a strong hydrophobic association feature.

3.3 Thermogravimetric analysis of polymers

As shown in Fig. 10, the mass loss of polymers can be divided into three stages: (1) 8% mass loss between 30–274 °C, (2) 26% mass loss between 274–359 °C, and (3) 29% mass loss when the temperature rises from 359 °C to 727 °C. The polymer is very stable in the temperature range of 30–274 °C, and test results show that the decomposition temperature of PHAAO is 287 °C. So, it can be used at 160 °C.

3.4 Leak plugging performance test

In order to verify the influence of the polymer on the loss of spacer fluid and the overall pressure strength, a medium
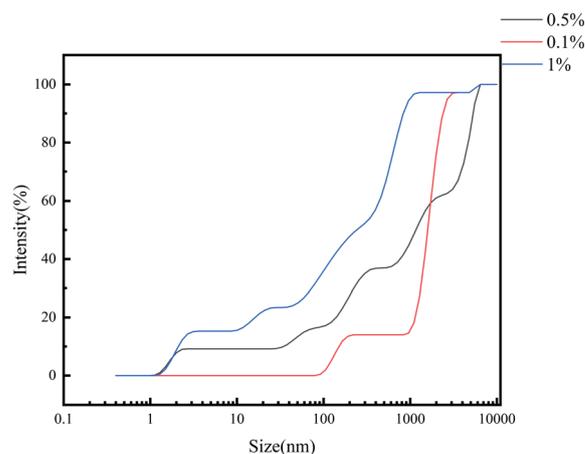

Fig. 8 Apparent viscosity of different concentration of PHAAO.

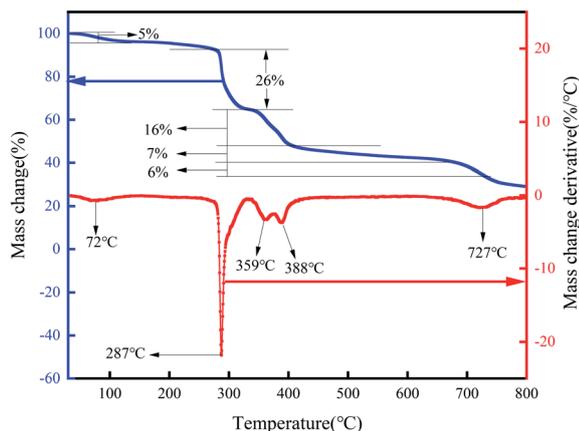Fig. 9 Cumulative fraction of scattered light intensity of polymers with different concentrations.

Fig. 10 TG and DTG curves of PHAAO solid.
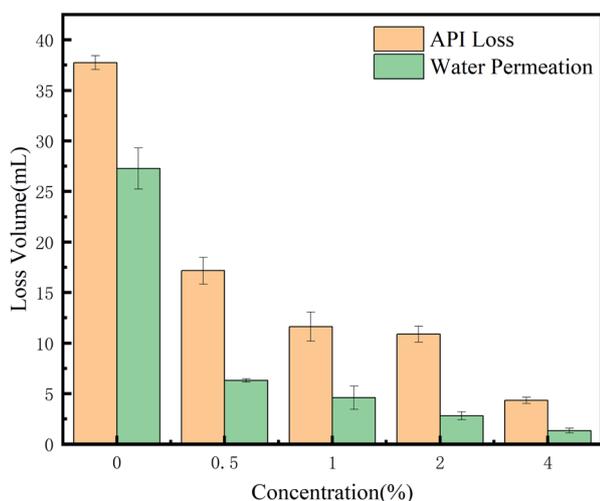

Fig. 11 API water loss test and filter cake water penetration test.

shows that the addition of 0.5 wt% PHAAO can significantly reduce water loss. When the dosage of the polymer PHAAO increases to 4 wt%, the water loss is only 10.8 mL. The change of water loss has a turning point at the critical association concentration of 1 wt%, because a large number of association network structures generate in the polymer at this concentration and the pores are effectively blocked. It also indicates the spacer fluid has a good ability to control free water.[25] The ordinate on the right of Fig. 11 shows the change of water penetrating through the filter cake within 30 min at 0.69 MPa. It can be seen that the water penetration of the filter cake has a similar change to the API loss and the water penetration is smaller because the filter cake is very dense. The tests demonstrate the filter cake under pressure has a very dense structure that prevents subsequent flow through the well from permeating into the fracture and prevents further leakage of microfractures and micropores.

It can be seen from Table 1 that when the PHAAO content reaches 1 wt%, the flow index n decreases while the consistency coefficient K increases sharply. This result indicates that although a higher content of PHAAO has a greater influence on the density of the filter cake and fills the pores better, the influence of its rheology should also be considered.

3.4.2 Loading capacity test under high temperature. The spacer fluid formula in Table 2 is water + a certain mass of plugging single-agent +4% suspension stabilizer DRY-S2 + 66% barite. As shown in Table 1, there is no loading capacity when rigid bridging material or PHAAO is used alone, proving that high bearing plugging requires the combination of bridging material, fiber material and ultra-low permeability agent. The experiment in Fig. 12 is to maintain nitrogen pressure at 5 MPa for 30 min and compare the influence of the polymer with different additives on the cumulative loss of spacer. Table 3 is to test the maximum loading capacity of spacer fluid after 30 min. As can be seen from Fig. 12, the cumulative loss within 30 min at 5 MPa is 15 mL when the PHAAO content is only 0.5 wt%, and the maximum loading capacity at 160 °C reaches 5 MPa. When

pressure water loss gauge and ultra-low permeability test were used respectively. The spacer fluid formula used was water + a certain mass fraction of polymer +1% 36-mesh walnut shell +1% lignin fiber +4% suspension stabilizer DRY-S2+66% barite.

3.4.1 Ultra-low permeability test. In order to verify the ultra-low permeability of the polymer in the spacer fluid filter cake, an API water loss test was carried out on the spacer fluid and water permeability tests were carried out on the filter cake obtained from the water loss test, as shown in Fig. 11. The figure

Table 2 Plugging ability test of a single agent at room temperature

Additive; mass/wt%	Loading capacity/MPa	Cumulative loss/mL
PHAAO; 4	0	Loss
Walnut shell; 12	0	Loss
Lignin fiber; 2	0	Loss

Table 1 Rheological parameters changing with concentration

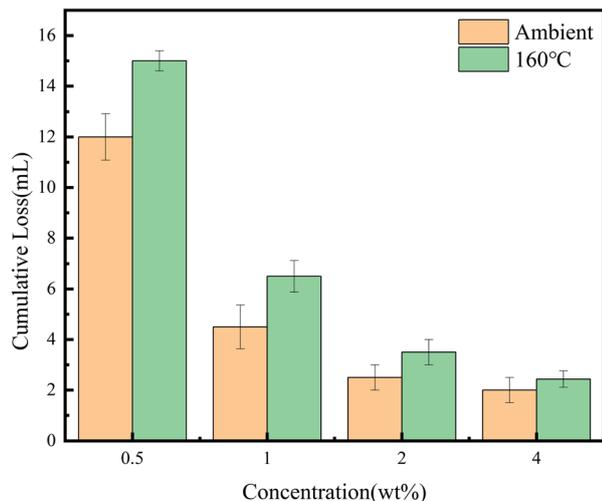| Concentration/wt%	Viscometer readings at the different rotational speed						n	K/Pa S^n	R^2
	θ_3	θ_6	θ_{100}	θ_{200}	θ_{300}	θ_{600}			
0	2.2	3.45	36.6	58.1	79.6	127.85	0.71	0.48	0.9995
0.5	2.1	3.35	42.85	68.6	90.85	144.85	0.69	0.63	0.9991
1	2.85	4.6	51.1	83.5	107.95	169	0.67	0.86	0.9988
2	4.75	7.7	71.25	115.7	147.35	227.35	0.64	1.35	0.9988
4	9.35	18.25	123.35	193.7	247.7	369	0.61	2.81	0.9989

Fig. 12   Effect of polymer addition on cumulative loss.

Fig. 13   Mechanism of plugging process.

its content is 1 wt%, the cumulative loss within 30 min at 5 MPa is only 4.5 mL, far less than that of 0.5 wt%. And its maximum bearing capacity at 160 °C reaches 6 MPa. The maximum pressure loading capacity of the spacer fluid exceeded 6.5 MPa at 4 wt% polymer.

It can be seen from the results that the polymer also plays a significant role in reducing leakage under high temperature and high pressure. The synergistic effect of the polymer, rigid bridge material and fiber material enables the spacer fluid to have a good high temperature plugging performance. Walnut shell has high compressive strength and strong thermal stability. It is insoluble in acid and alkali, being friendly to the environment. Lignin fiber is an important part of road-building materials with good toughness and heat resistance.[26] According to the thermal weight loss test results, partial side-chain removal occurred after 274 °C, which proved that the polymer still had strong association characteristics after curing at 160 °C. Besides, lignin and walnut shell would not degrade at 160 °C. Their excellent high-temperature resistance makes the pressure loading capacity and anti-leakage capacity of the spacer fluid not being weakened too much after high-temperature curing.

The plugging process mechanism is shown in Fig. 13. As the spacer fluid passes through the crack, rigid bridging materials on the network form a bridge to narrow the apertures, and then the filter cake is further densified by the lignin wrapping with walnut shell. Finally, the polymer continues to fill the filter cake until the pores of the filter cake are completely sealed and the liquid stops leaking. The fibers are interlaced and wound with each other, forming a high-strength three-dimensional network with walnut shells, and compounded with the hydrophobic associating polymer. So, the spacer fluid has the characteristics of high-temperature resistance, high-pressure resistance and low permeability. The addition of the polymer increases the pressure loading capacity of the spacer fluid due to the effective sealing of micropores by the polymer. It can form strong hydrogen bonding with lignin fiber. The loading capacity improves because of the winding of the lignin and walnut shell and the hydrogen bonding interaction between the polymer and lignin fibers. Although the cumulative loss can be further reduced when the polymer content is 4 wt%, it can be seen from Table 1 that the flow index decreases and the consistency coefficient increases excessively, which is unfavorable in actual pumping applications. When the dosage is only 1 wt%, good rheological properties and plugging pressure can be obtained.

3.5 Compatibility test of the spacer fluid

According to the national standard, the compatibility of spacer fluid and cement slurry should be tested. In the cementing operation, it is required that flash coagulation and flocculation should not occur when mixing spacer fluid and cement slurry, otherwise the spacer fluid will affect the flow of cement slurry and does harm to the cementing quality. The rheological properties and thickening properties of the mixture were tested. Cement formula: cement +2% fluid loss agent +44% fresh water, spacer fluid formula: water +1% polymer +1% 36-mesh walnut shell +1% lignin fiber +4% suspension stabilizer DRY-S2 +66% barite.

3.5.1 Rheological compatibility with cement slurry. As can be seen from Tables 4 and 5, the rheological compatibility of spacer fluid and cement slurry is good. When the spacer fluid is mixed with cement slurry, the fluidity of the slurry is 18–23 cm at room temperature and 22 cm at 93 °C. The fluidity of the

Table 3   Influence of polymer content on maximum loading capacity

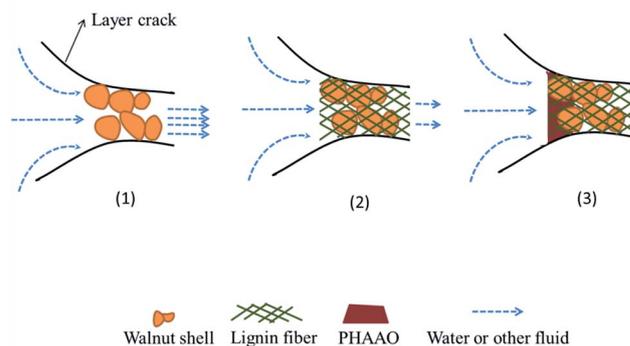| PHAAO/wt%	Temperature/°C	Loading capacity maximum/MPa
0	Ambient	0, loss
	160	0, loss
0.5	Ambient	5
	160	5
1	Ambient	6
	160	6
2	Ambient	6.5
	160	6.5
4	Ambient	>6.5
	160	>6.5

Table 4 Rheological compatibility with cement slurry at ambient temperature

Cement/spacer (v/v)	Viscometer readings at different rotational speed						n	K/Pa S^n	R^2	Fluidity/cm
	θ_3	θ_6	θ_{100}	θ_{200}	θ_{300}	θ_{600}				
100/0	7.2	10.1	29.45	39.85	50.45	76.95	0.64	0.42	0.991	8
95/5	18.35	21.45	41.35	49.85	57.35	79.85	0.55	0.73	0.972	17.5
75/25	2.7	3.75	20.25	32.25	45.35	79.85	0.84	0.12	0.998	24

Table 5 Rheological compatibility with cement slurry at 93 °C

Cement/spacer (v/v)	Viscometer readings at different rotational speed						n	K/Pa S^n	R^2	Fluidity/cm
	θ_3	θ_6	θ_{100}	θ_{200}	θ_{300}	θ_{600}				
100/0	10.1	15.45	67.2	83.2	94.7	91.2	0.22	17.1	0.916	13
95/5	8.85	10.35	34.7	43.5	64.6	75.35	0.44	1.89	0.979	24
75/25	0.7	1.25	14.5	25.45	33.35	60.35	0.80	0.12	0.999	28

slurry is higher than that of pure cement at both temperatures. The fluidity index of the mixture at room temperature and high temperature is greater than 0.6, and the consistency coefficient is less than one.

3.5.2 Consistency of thickening. As can be seen from Fig. 14, 15 and 16, the spacer fluid is well compatible with the cement slurry when the cement is thickening. The mixtures of volume ratios of 5/95 and 25/75 did not shorten the thickening time and the curve in the early stage was relatively stable, without bulge and entrapment phenomenon. The results indicate the spacer fluid would not cause flash coagulation and flocculation of cement slurry.

To sum up, the rheological compatibility and thickening compatibility of spacer fluid and cement slurry are good.

3.6 Study on membrane formation mechanism

Scanning electron microscopy (SEM) was used to observe the influence of the polymer PHAAO addition on the morphology of the filter cake of the spacer fluid. The addition amount of

polymer PHAAO was 1 wt%. As shown in Fig. 17, the spacer fluid without PHAAO and that with PHAAO have a great difference in the apparent morphology of the filter cake. In Fig. 17(a), there are many tiny voids in the spacer fluid filter cake without PHAAO, and the particles are disordered and no certain structure is formed. As shown in Fig. 17(b), PHAAO fills a large amount of the microstructure of the spacer fluid cake, making the filter cake being very smooth and compact with almost no pores. It has been pointed out in the literature that ultra-low permeability agents used in ultra-low permeability drilling fluids have similar working mechanisms.[27] When the polymer concentration reaches the critical association concentration, the intermolecular association becomes the dominant interaction. Through attachment and association, the polymers form a large number of grid structure. They assemble to be micelles on the pore surface. So low permeable formation is produced to effectively fill the gaps between other solid components, and the water loss of spacer fluid is greatly reduced.

Chart 2 shows the molecular structure of lignin which contains groups such as benzene ring, methoxy group and
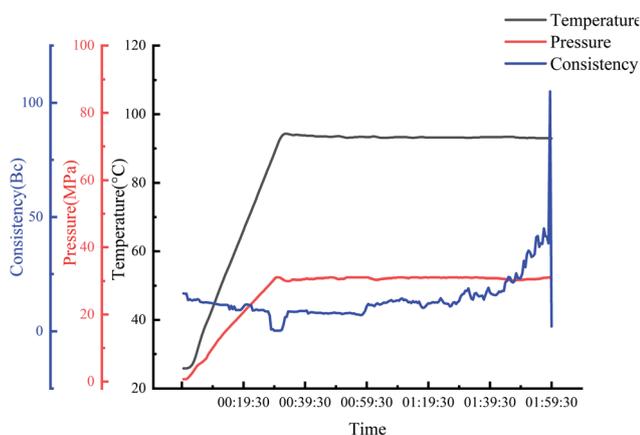

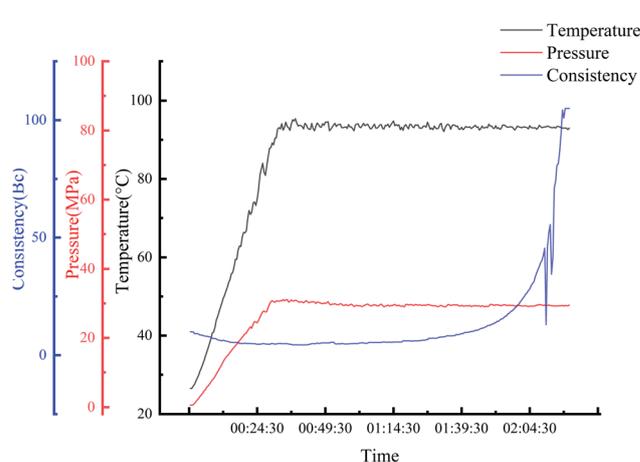**Fig. 14** Thickening curve of cement/spacer fluid volume ratio of 100/0.

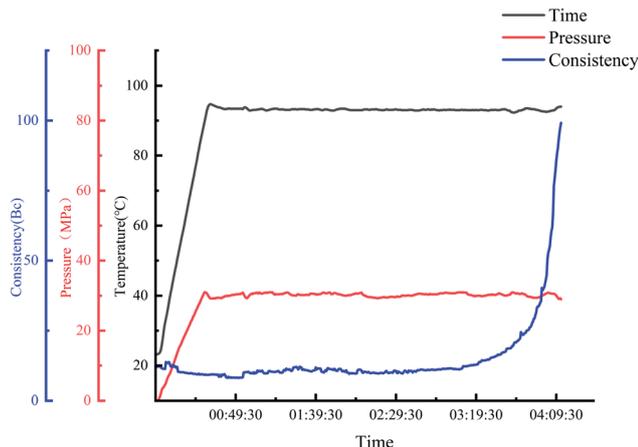**Fig. 15** Thickening curve of cement/spacer fluid volume ratio of 95/5.

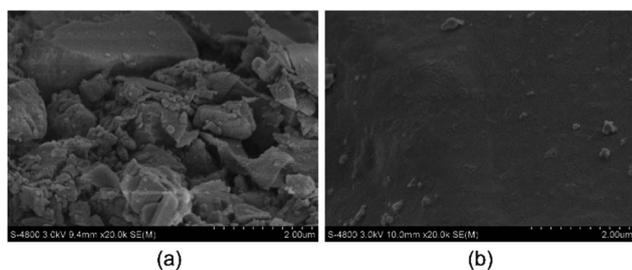**Fig. 16** Thickening curve of cement/spacer fluid volume ratio of 75/25.

Fig. 17 (a) Image of filter cake from plugging spacer without PHAAO (b) image of filter cake from plugging spacer with PHAAO.

hydroxyl group. Methoxy and benzene rings are non-polar groups and can form hydrophobic associations with other non-polar groups, while hydroxyl groups can form hydrogen bonds with nitrogen atoms. The spacer fluid system environment is weakly acid where the amino groups on the polymer will be protonated into NH_3^+ and can form cationic–π bonds with the benzene ring on the lignin.[28–31] As shown in Fig. 18, the methoxy groups on lignin fibers form hydrophobic associations
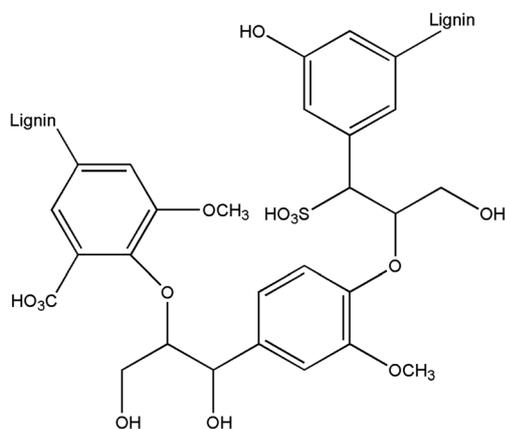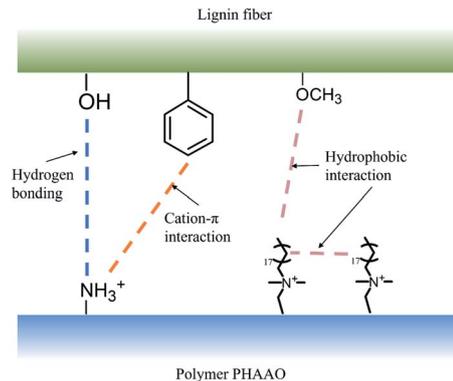

Chart 2 Structural formula of lignin.

Fig. 18 Interaction forces between lignin fiber and polymer.

with the alkyl long side chain on the polymer, the hydroxyl groups can form hydrogen bonds with the amino groups on acrylamide and the benzene rings on lignin fibers can form cationic–π bonds with the amino groups. The polymers were able to adhere tightly to the cake surface because of the interaction between the polymers together with the interaction between the polymers and lignin. One research[32] mentioned that there is hydrogen bonding between lignin and polyacrylamide. Adding lignin to the mixture of polypropylene and polyacrylamide can significantly improve the compatibility between polypropylene and polyacrylamide. Another article[33] mentioned that hydrophobic interaction, electrostatic interaction and cationic–π interaction exist between lignin nanofilms and amino groups, which are consistent with the findings in this paper. It can be seen that there are interactions between polymers and polymers as well as between lignin and polymer. These interactions enable polymers to form the dense membrane through hydrophobic association and attach tightly to lignin fibers, resulting in the effect shown in Fig. 17(b).

4   Conclusion

(1) The hydrophobic associating polymer PHAAO was successfully synthesized, and its thermal decomposition temperature is 287 °C. Fluorescence and ultraviolet spectra confirmed the existence of the expected hydrophobic microregion in an aqueous solution with a critical association concentration of 1%. The degree of association increased with the increase of PHAAO concentration. The dynamic light scattering analysis shows that the polymer has a strong association property.

(2) Through API loss test and loading capacity test under high temperature prove that the polymer can make plugging spacer fluid form ultra-low permeability membrane. The synergistic effect of walnut shell, lignin fiber and polymer make the spacer fluid has the characteristics of high-temperature resistance, high-pressure resistance and ultra-low filtration loss. After curing at room temperature and 160 °C, only 1% polymer content can make the sealing pressure strength of spacer fluid for 1 mm crack reach more than 6 MPa. Meanwhile, the spacer fluid does not affect the flow and thickening properties of cement slurry.

Author contributions

Zhaofeng Xue-data curation, formal analysis, investigation, methodology, writing – original draft. Miaomiao Hu-formal analysis, conceptualization, writing – review & editing. Xia Miao-funding acquisition, conceptualization. Long Zang-investigation Jintang Guo-project administration, writing – review & editing, supervision, conceptualization.

Conflicts of interest

There are no conflicts to declare.

Acknowledgements

References

1 T. Xuechen, Y. Hongbin, G. Yongbo, *et al.*, Preparation of a micron-size silica-reinforced polymer microsphere and evaluation of its properties as a plugging agent, *Colloids Surf., A*, 2018, **547**, 8–18.

2 H. Xianbin, S. Jinsheng, L. Kaihe, *et al.*, Application of core-shell structural acrylic resin/nano-SiO2 composite in water-based drilling fluid to plug shale pores, *J. Nat. Gas Sci. Eng.*, 2018, **55**, 418–425.

3 G. Liu, C. Luo and B. Wang, The Research of Polymer Film-Forming Plugging Agent for Drilling Fluid, *Open J. Yangtze Oil Gas*, 2019, **4**(4), 8.

4 X. Shi and X. Yue, Migration and plugging mechanisms of self-aggregated microspheres as a novel profile control, *J. Petrol. Sci. Eng.*, 2020, **184**, 106458.

5 X. Yu, W. Pu, D. Chen, J. Zhang, F. Zhou, R. Zhang and S. Gu, Degradable cross-linked polymeric microsphere for enhanced oil recovery applications, *RSC Adv.*, 2015, **5**(77), 62752–62762.

6 J. G. Xu, Z. Qiu, Z. Xin, *et al.*, A polymer microsphere emulsion as a high-performance shale stabilizer for water-based drilling fluids, *RSC Adv.*, 2018, **8**(37), 20852–20861.

7 H. Yang, L. Hu, C. Chen, *et al.*, Synthesis and plugging behavior of fluorescent polymer microspheres as a kind of conformance control agent in reservoirs, *RSC Adv.*, 2018, **8**(19), 10478–10488.

8 B. Xie and L. Zheng, New drilling fluid plugging agent based on hydrophobic associating polymer, *Oil Drill. Prod. Technol.*, 2015, **37**(5), 5.

9 Y. Xue. *Study on action mechanism and application of ultra-low permeability drilling fluid*. China University of Petroleum, East China, 2008.

10 J. Sun, Review of ultra-low permeability drilling fluid technology abroad, *Drill. Fluid Completion Fluid*, 2005, **22**(1), 3.

11 Ke Liu. *Experimental study of ultra-low invasive drilling fluid*. China university of petroleum, Beijing, 2006.

12 M. G. Wessels and A. Jayaraman, Self-assembly of amphiphilic polymers of varying architectures near attractive surfaces, *Soft Matter*, 2020, **16**(3), 623–633.

13 Y. Cao, Y. Zheng and G. Pan, Radical generation process studies of the cationic surfactants in ultrasonically irradiated emulsion polymerization, *Ultrason. Sonochem.*, 2008, **15**(4), 320–325.

14 H. Zhang, M. Hu, Y. Xu, *et al.*, Inhibitory effects of functionalized polycarboxylate retarder on aberrant thickening phenomena of oil well cement at high temperature, *Constr. Build. Mater.*, 2021, **274**, 121994.

15 J. Zhong, Y. Guo, J. Liu, *et al.*, The synthesis conditions of micellar polymerization were determined by steady state fluorescence quenching method, *Appl. Chem. Ind.*, 2012, **41**(3), 4.

16 W. Luo, B. Jiang, L. Cheng, *et al.*, Application of fluorescent probe technique in self-assembly of polymer, *Prog. Chem.*, 2013, **10**, 1713–1725.

17 A. Roa, A. Gfo, B. So, *et al.*, Determination of a critical separation concentration for associative polymers in porous media based on quantification of dilute and semi-dilute concentration regimes, *J. Mol. Liq.*, 2020, **317**, 114142.

18 K. C. Tam, W. K. Ng and R. D. Jenkins, Rheological Properties of Hydrophobically Modified Polyelectrolyte Systems: Concentration Effects, *J. Appl. Polym. Sci.*, 2006, **102**(6), 5166–5173.

19 R. Zhu, Y. Feng and P. Luo, Net Contribution of Hydrophobic Association to the Thickening Power of Hydrophobically Modified Polyelectrolytes Prepared by Micellar Polymerization, *Macromolecules*, 2020, **53**(4), 1326–1337.

20 G. Li, Y. Shen, P. Li, *et al.*, Study on solution properties of surfactant fluorine-containing monomer acrylamide copolymer, *Acta Polym. Sin.*, 2010, **1**(3), 347–351.

21 X. Shi and X. Yue, Migration and plugging mechanisms of self-aggregated microspheres as a novel profile control, *J. Petrol. Sci. Eng.*, 2020, **184**, 106458.

22 X. Xia, J. Guo, S. Liu, *et al.*, Research of Nanosilica Particles Grafted with Functional Polymer Used as Fluid Loss Additive for Cementing under Ultra-high Temperature, *Mater. Sci. Forum*, 2016, **847**, 497–504.

23 X. Xia, J. Guo, Y. Feng, *et al.*, Hydrophobic associated polymer grafted onto nanosilica as a multi-functional fluid loss agent for oil well cement under ultrahigh temperature, *RSC Adv.*, 2016, **6**(94), 91728–91740.

24 B. Cao, M. Chen, P. Luo, W. Wangkun and S. Li, The critical association concentration of hydrophobic associating polymer solution, *J. Xi'an Shiyou Univ., Nat. Sci. Ed.*, 2008, **04**, 40–42+48+4.

25 M. Li, H. Ou, H. Liu, *et al.*, Research on the impact of inorganic components on the performance of a novel self-solidified spacer fluid, *J. Nat. Gas Sci. Eng.*, 2016, **33**, 315–323.

26 J. Yang, Y. C. Ching and C. H. Chuah, Applications of Lignocellulosic Fibers and Lignin in Bioplastics: A Review, *Polymers*, 2019, **11**(5), 751.

27 B. Xie. *Plugging drilling fluid based on hydrophobic associated polymer*. China university of petroleum, Beijing. 2017.

28 Y. Zhu, M. Tang, H. Zhang, *et al.*, Water and the Cation-π Interaction, *J. Am. Chem. Soc.*, 2021, **143**(31), 12397–12403.

29 T. Song, H. Lei, F. Cai, *et al.*, Supramolecular Cation-π Interaction Enhances Molecular Solar Thermal Fuel, *ACS Appl. Mater. Interfaces*, 2022, **14**(1), 1940–1949.

30 X. Liu, S. Sheng, H. Yang, *et al.*, Uniform, Anticorrosive, and Antiabrasive Coatings on Metallic Surfaces for Cation–Metal and Cationπ Interactions, *ACS Appl. Mater. Interfaces*, 2020, **12**(34), 38638–38646.

31 A. Dennis, The Cation−π Interaction, *Acc. Chem. Res.*, 2013, **46**(4), 885–893.

32 B. Tian, J. Li, Z. Li, *et al.*, Preparation of polypropylene with high melt strength by wet reaction blending of lignin, *J. Appl. Polym. Sci.*, 2022, **139**(1), 51224.

33 L. S. Yoon, *et al.*, pH-Dependent interaction mechanism of lignin nanofilms, *Nanoscale*, 2021, **13**, 19568–19577.